Design of ultra-compact triplexer with function-expansion based topology optimization

Zejun Zhang,[1,3] **Yasuhide Tsuji,**[1,*] **Takashi Yasui,**[2,4] **and Koichi Hirayama**[2,5]

[1]*Division of Information and Electronic Engineering, Muroran Institute of Technology, Muroran, 050-8585, Japan*
[2]*Department of Electrical and Electronic Engineering, Kitami Institute of Technology, Kitami, 090-8507, Japan*
[3]*12054072@mmm.muroran-it.ac.jp*
[4]*yasui@mail.kitami-it.ac.jp*
[5]*hirakc@mail.kitami-it.ac.jp*
[*]*y-tsuji@mmm.muroran-it.ac.jp*

Abstract: In this paper, in order to optimize wavelength selective photonic devices using the function-expansion-based topology optimization method, several expansion functions are considered and the influence on the optimized structure based on each expansion function was investigated. Although the Fourier series is conventionally used in the function-expansion-based method, the optimized structure sometimes has a complicated refractive index distribution. Therefore, we employed a sampling function and a pyramid function to obtain a simpler structure through the optimal design. A triplexer was designed by using our method, and the comparison between the optimized structures based on the three expansion functions was also discussed in detail.

OCIS codes: (230.7390) Waveguides, planar.

References and links

1. T. T. Shih, Y. D. Wu, and J. J. Lee, "Proposal for compact optical triplexer filter using 2-D photonic crystals," IEEE Photon. Technol. Lett. **21**(1), 18–20 (2009).
2. L. Zhang, P. Chen, and Y. Shi, "Design and experimental verification of all waveguide type triplexers using cascaded MMI coupler," Opt. Quant. Electron. (to be published).
3. X. Lin, T. Lang, and J. He, "Design analysis and experimental verification of cross-order AWG triplexer based on silica-on-silicon," J. Lightwave Technol. **29**(9), 1407–1413 (2011).
4. J. Zou, X. Jiang, X. Xia, T. Lang, and J. He, "Ultra-compact birefringence-compensated arrayed waveguide grating triplexer based on silicon-on-insulator," J. Lightwave Technol. **31**(12), 1935–1940 (2013).
5. V. Jerabek, K. Busek, V. Prajzler, D. Mares, and R. Svoboda, "The design of polymer planar optical triplexer with MMI filter and directional coupler," Radioengineering **22**(4), 1307–1314 (2013).
6. J. Jiang, J. Cai, G. P. Nordin, and L. Li, "Parallel microgenetic algorithm design for photonic crystal and waveguide structures," Opt. Lett. **28**(23), 2381–2383 (2003).
7. Y. Sakamaki, T. Saida, T. Hashimoto, and H. Takahashi, "New optical waveguide design based on wavefront matching method," J. Lightwave Technol. **25**(11), 3511–3518 (2007).
8. J. S. Jensen and O. Sigmund, "Systematic design of photonic crystal structures using topology optimization: Low-loss waveguide bends," Appl. Phys. Lett. **84**(12), 2022–2024 (2004).
9. J. S. Jensen, O. Sigmund, L. H. Frandsen, P. I. Borel, A. Harpoth, and M. Kristensen, "Topology design and fabrication of an efficient double 90° photonic crystal waveguide bend," IEEE Photon. Technol. Lett. **17**(6), 1202–1204 (2005).

#229351 - $15.00 USD Received 18 Dec 2014; revised 31 Jan 2015; accepted 1 Feb 2015; published 9 Feb 2015

10. R. Matzen, J. S. Jensen, and O. Sigmund, "Topology optimization for transient response of photonic crystal structures," J. Opt. Soc. Amer. B **27**(10), 2040–2050 (2010).
11. F. Wang, J. S. Jensen, and O. Sigmund, "Robust topology optimization of photonic crystal waveguides with tailored dispersion properties," J. Opt. Soc. Amer. B **28**(3), 387–397 (2011).
12. L. Frandsen, Y. Elesin, L. Frellsen, M. Mitrovic, Y. Ding, O. Sigmund, and K. Yvind, "Topology optimized mode conversion in a photonic crystal waveguide fabricated in silicon-on-insulator material," Opt. Express **22**(7), 8525–8532 (2014).
13. H. Men, K. Y. K. Lee, R. M. Freund, J. Peraire, and S. G. Johnson, "Robust topology optimization of three-dimensional photonic-crystal band-gap structures," Opt. Express **22**(19), 22632–22648 (2014).
14. Y. Tsuji, K. Hirayama, T. Nomura, K. Sato, and S. Nishiwaki, "Design of optical circuit devices based on topology optimization," IEEE Photon. Technol. Lett. **18**(7), 850–852 (2006).
15. Y. Tsuji and K. Hirayama, "Design of optical circuit devices using topology optimization method with function-expansion-based refractive index distribution," IEEE Photon. Technol. Lett. **20**(12), 982–984 (2008).
16. K. Fujimoto, Y. Tsuji, K. Hirayama, T. Yasui, S. Sato, and R. Kijima, "A study on topology optimization of optical circuits consisting of multi-materials," J. Lightwave Technol. **30**(13), 2210–2215 (2012).
17. T. Yasui, Y. Tsuji, J. Sugisaka, and K. Hirayama, "Design of three-dimensional optical circuit devices by using topology optimization method with function-expansion-based refractive index distribution," J. Lightwave Technol. **31**(23), 3765–3770 (2013).
18. Y. Tsuji and M. Koshiba, "Finite element method using port truncation by perfectly matched layer boundary conditions for optical waveguide discontinuity problems," J. Lightwave Technol. **20**(3), 463–468 (2002).
19. D. Dimitropoulos, V. Raghunathan, R. Claps, and B. Jalali, "Phase-matching and nonlinear optical processes in silicon waveguide," Opt. Express **12**(1), 149–160 (2004).

1. Introduction

With the popularity of the Internet in recent years, the demand for high-speed and large-capacity optical communication system has been further increased. In order to achieve the high-speed and large-capacity optical communication system, the demand for high-performance optical devices has also been increased. Moreover, the high-performance optical devices, such as triplexer, polarization converter etc., have been developed by improving the existing structures based on analytical or numerical analysis.

Triplexer plays an important role in the fiber-to-the-home (FTTH) network, which represents the fastest growing telecommunication sector so far. The triplexer is generally used as a multiplexer or a demultiplexer for three kinds of wavelength channels, *i.e.* 1.31 μm, 1.49 μm and 1.55 μm, respectively. Several papers on designing and fabricating the triplexer have appeared recently [1–5]. In 2009, Shih *et al*. proposed a triplexer using 2-D photonic crystals (PC) whose transmission efficiency is larger than 94% [1]. Due to low polarization dependence, relatively large bandwidth and compactness, multimode interference (MMI) based triplexer has been proposed [2]. However, the triplexer with three cascaded MMI sections has a complicated structure and a large device size. A silicon-nanowire-based arrayed waveguide grating (AWG) triplexer, which has a footprint of 0.18×0.12 mm^2 , has been put forward in 2013 [4].

In recent years, with the development of high-speed computer and numerical simulation techniques, several kinds of researches on the automatic optimum design have been reported, such as genetic algorithms (GA) [6], wavefront matching method (WFM) [7], and topology optimization [8–17]. The topology optimization method can automatically generate the structure which realizes the desired characteristics. In contrast to GA, the topology optimization has a faster convergence to the optimal solution due to the method based on sensitivity analysis. Furthermore, topology optimization using finite element method (FEM) [18] can also design the reflection-type photonic device which cannot be processed by WFM. As we know, the density method is widely used to express the index distribution of design region in topology optimization. However, the continuous density parameters which are known as gray area can lead to the design region with an intermediate value between the usable materials.

In our research, we designed an ultra-compact triplexer using topology optimization with design region of $2\ \mu\text{m} \times 2\ \mu\text{m}$ and $4\ \mu\text{m} \times 4\ \mu\text{m}$, respectively. In order to avoid the gray area, we

#229351 - $15.00 USD Received 18 Dec 2014; revised 31 Jan 2015; accepted 1 Feb 2015; published 9 Feb 2015

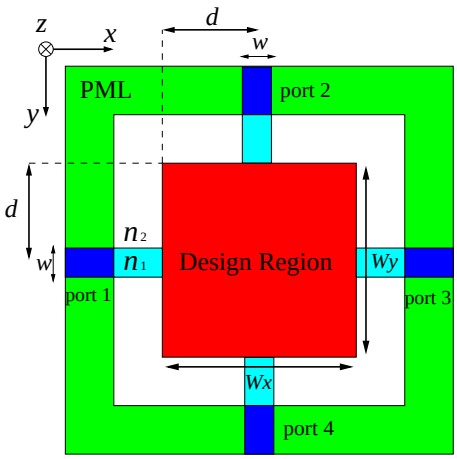

Fig. 1. A triplexer to be topology optimized.

employed the function-expansion method [14–17] to express the refractive index distribution in the design region. In the function-expansion method, a Fourier series was used to express the refractive index distribution so far. However, in that case, the finally obtained optimized structure tends to be complicated. Therefore, in this paper, we adopted the function-expansion with two kinds of localized functions to avoid the complicated structure, *i.e.* a sampling function and a pyramid function. In addition, the obtained characteristics and structures of triplexer by using different functions were also compared and discussed in detail.

The paper is organized as follows. In the next section, the topology optimization with function-expansion method has been discussed in detail. Following that, two 2-D deign examples of triplexer with different expansion functions and different design regions are given, then a quasi 3-D design example which considering the variation of material index against different wavelengths [19] is investigated. Finally, the conclusions and future works.

2. Topology optimization with function-expansion method

2.1. Expression for refractive index distribution in the design region

In our research, we consider a design problem of triplexer whose design area consists of two materials with different refractive indices of n_1 and n_2, as shown in Fig. 1. The design region is surrounded by the perfectly matched layer (PML) to avoid the complicated modal expansion for the input and output waveguides [18]. A beam of three-wavelength multiplexed light is launched into port 1, and through the optimal design region of size W_x by W_y, light of each wavelength separates into different ports (ports 2 to 4), respectively.

In this paper, the triplexer is designed only using two kinds of materials, and the refractive index distribution of the design region can be expressed by an analytical function $\xi(x,y)$ as follows:

$$n^2(x,y) = n_2^2 + (n_1^2 - n_2^2)H(\xi(x,y)) \tag{1}$$

where n_1 and n_2 ($n_1 > n_2$) are the refractive indices of two considered materials, respectively. The value of function $H(\xi)$ takes 0 or 1 according to the value of ξ, and $n(x,y)$ is equivalent to either n_1 or n_2 depending on the value of $\xi(x,y)$.

Here, we design the function $H(\xi)$ as follows to make it possible to take the differential of

#229351 - $15.00 USD Received 18 Dec 2014; revised 31 Jan 2015; accepted 1 Feb 2015; published 9 Feb 2015

$H(\xi)$ in the sensitivity analysis

$$H(\xi) = \begin{cases} 0 & (\xi \le -h) \\ \frac{1}{2}\left(\frac{\xi+h}{h}\right)^2 & (-h < \xi < 0) \\ 1-\frac{1}{2}\left(\frac{\xi-h}{h}\right)^2 & (0 \le \xi < h) \\ 1 & (\xi \ge h) \end{cases} \tag{2}$$

where h is a quantity that has been introduced into the continuous function $H(\xi)$. If $|\xi(x,y)| < h$, the value of $n(x,y)$ will be an intermediate refractive index between the two kinds of materials used in the waveguide and the gray area appears, which makes the optimized structure difficult to be fabricated. In order to suppress the gray area, h should take a small value as much as possible. The optimized structure without any gray area can be achieved when $h \to 0$.

Generally, the refractive index distribution of the design region can be determined by function $\xi(x,y)$, which is expressed in the form of the superposition of some analytical functions $f_i(x,y)$. Here $\xi(x,y)$ is given by

$$\xi(x,y) = \sum_{i=1}^{N} c_i f_i(x,y). \tag{3}$$

Referring to [15], $\xi(x,y)$ can be expressed by using a Fourier series as follows:

$$\xi(x,y) = \sum_{i=0}^{N_x-1} \sum_{j=-N_y}^{N_y-1} (a_{ij}\cos\theta_{ij} + b_{ij}\sin\theta_{ij}) = \sum_{i=0}^{N_x-1} \sum_{j=-N_y}^{N_y-1} (a_{ij} f_{ij}(x,y) + b_{ij} g_{ij}(x,y)) \tag{4}$$

$$\theta_{ij} = \frac{2\pi i}{L_x}x + \frac{2\pi j}{L_y}y \tag{5}$$

where N_x, $2N_y$ are the numbers of expansion functions along x and y directions. The values of L_x and L_y are set to be greater than W_x and W_y, respectively. However, since the trigonometric function has a constant amplitude in the entire design region, the effect which caused by changing some local area would extend to all the design region. The finally obtained structure is sometimes complicated, especially in the strongly guiding design problem with many local optimal structures. Therefore, in this paper, in order to avoid the complicated final structure, we optimized the triplexer by using a localized function, such as sampling function or pyramid function, to express the refractive index distribution of the design region. Here, $\xi(x,y)$ is represented by the function expansion items in x- and y-direction, respectively,

$$\xi(x,y) = \sum_{i=0}^{N_x} \sum_{j=0}^{N_y} a_{ij} f\left(\frac{x-x_i}{\Delta x}\right) f\left(\frac{y-y_j}{\Delta y}\right) = \sum_{i=0}^{N_x} \sum_{j=0}^{N_y} a_{ij} f_{ij}(x,y) \tag{6}$$

with

$$\begin{array}{ll} f(\zeta) = \mathrm{sinc}(\pi\zeta), & \text{for sampling function} \\ f(\zeta) = (1-|\zeta|)\{u(\zeta-1)-u(\zeta+1)\}, & \text{for pyramid function} \end{array} \tag{7}$$

where (x_i, y_i) is the coordinate of a sample point (i, j), Δx and Δy are the sampling intervals in x- and y-direction, respectively, and $u(\zeta)$ is a step function. Figure 2 shows the basis functions and the structure representation of the Fourier series, sampling function and pyramid function, respectively. The Figs. on the left side show the 3-D distribution of each function, the center Figs. represent the cross-section view at $y = 0$ of each function, and the Figs. on the right side illustrate an example of $\xi(x,y)$ which is superposition of the basis functions. It can be seen that, in the Fourier series, the effect extends to the whole region when the amplitude of a basis function is changed. On the other hand, the influence range is limited in the two kinds of localized functions.

#229351 - $15.00 USD Received 18 Dec 2014; revised 31 Jan 2015; accepted 1 Feb 2015; published 9 Feb 2015

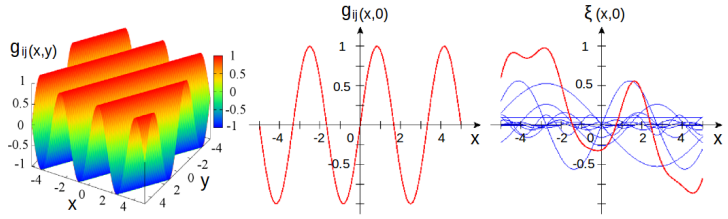

(a) Fourier series

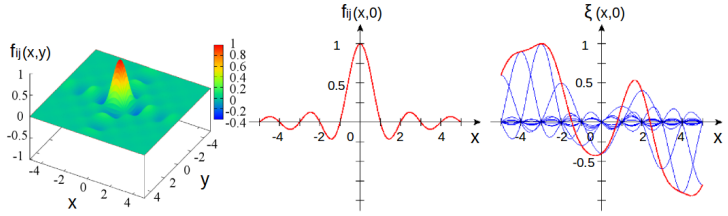

(b) Sampling function

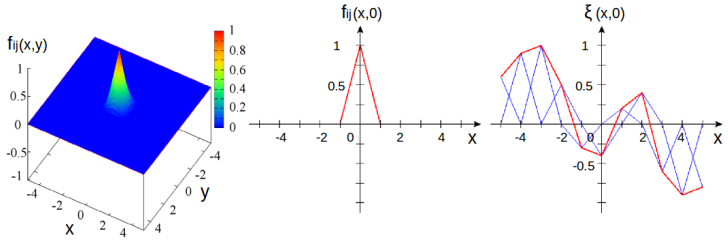

(c) Pyramid function

Fig. 2. Basis functions and the structure representation.

2.2. *Formulation by the finite element method*

Generally, it is difficult to expand the eigen modes for the input and output waveguides in an open system such as an optical waveguide. Here, we surround the design region by PML and evaluate the transmission characteristics of the optical devices by employing the FEM which can eliminate the need for modal expansion. The wave equation of a 2-D optical circuit with a uniform structure in z-direction can be obtained by Maxwell's equations, as follows:

$$\frac{\partial}{\partial x}\left(p\frac{\partial \Phi}{\partial x}\right)+\frac{\partial}{\partial y}\left(p\frac{\partial \Phi}{\partial y}\right)+k_0^2 q\Phi=0 \tag{8}$$

with

$$\begin{array}{llll} \Phi=E_z, & p=1, & q=n^2 & \text{for TE wave} \\ \Phi=H_z, & p=1/n^2, & q=1 & \text{for TM wave} \end{array} \tag{9}$$

where E_z and H_z are the z-direction components of electric and magnetic fields, respectively. And k_0 is the free space wave number. Dividing the whole analysis region into a number of second order triangular elements, the z-direction component Φ for electric or magnetic fields can be written as follows:

$$\Phi=\{N\}^T\{\Phi\}_e \tag{10}$$

where $\{\Phi\}_e$ is the vector value of Φ in each element node. $\{N\}$ is the shape function vector, and T means transpose. Applying the FEM described in [18], we can obtain a final matrix equation

#229351 - $15.00 USD Received 18 Dec 2014; revised 31 Jan 2015; accepted 1 Feb 2015; published 9 Feb 2015

as follows:

$$[P]\{\Phi\} = \{u\} \tag{11}$$

with

$$[P] = \sum_e \iint_e \left[p\frac{s_y}{s_x}\frac{\partial\{N\}}{\partial x}\frac{\partial\{N\}^T}{\partial x} + p\frac{s_x}{s_y}\frac{\partial\{N\}}{\partial y}\frac{\partial\{N\}^T}{\partial y} - k_0^2 q s_x s_y \{N\}\{N\}^T \right] dxdy \tag{12}$$

$$\{u\} = \sum_e{}' \int_e p\frac{s_y}{s_x}\{N\}_\Gamma \left(\frac{\partial\Phi_1}{\partial x} - \frac{\partial\Phi_2}{\partial x} \right) d\Gamma \tag{13}$$

where $\{N\}_\Gamma$ is the shape function vector at the incident plane Γ. Here, $\sum_e$ means the sum of all elements and $\sum_e{}'$ means the sum of elements which contact with the incident plane Γ. In addition, the field Φ in positive and negative region of x-direction for the boundary Γ are represented by Φ_1 and Φ_2, respectively. s_x and s_y are the parameters of PML [18].

2.3. Sensitivity analysis by the adjoint variable method

In the function-expansion-based topology optimization method, the desired characteristics of optical device in the design region can be achieved by continuously updating the coefficient c_i of Eq. (3). Since the objective function is always expressed by the scattering parameter S_{n1}, here, we defined S_{n1} as follows:

$$S_{n1} = \{\Phi\}^T\{g_n\} \tag{14}$$

with

$$\{g_n\} = [Q]\{\Phi_n\} \tag{15}$$

$$[Q] = \frac{c\beta_n}{k_0}\sum_{e_n}\int_{\Gamma_n} p\{N\}\{N\}^T d\Gamma_n \tag{16}$$

where vector $\{\Phi_n\}$ and β_n are the modal function and the propagation constant of the n-th input and output waveguides, respectively. And c represents the speed of light. The derivative of S_{n1} with respect to c_i has been calculated, and we represent $\partial S_{n1}/\partial c_i$ as follows:

$$\frac{\partial S_{n1}}{\partial c_i} = -\{\lambda_n\}^T\frac{\partial[P]}{\partial c_i}\{\Phi\} \tag{17}$$

with

$$[P]^T\{\lambda_n\} = \{g_n\} \tag{18}$$

We can obtain $\{\lambda_n\}$ by solving Eq. (18), and we can also efficiently calculate $\partial S_{n1}/\partial c_i$ by the product of the known vectors. Here, it is important to calculate $\partial n^2/\partial c_i$ in Eq. (17), and that can be written as follows:

$$\frac{\partial n^2}{\partial c_i} = f_i(x,y)(n_1^2 - n_2^2)H'(\xi). \tag{19}$$

2.4. Setting the gray area in optimization process

In the function-expansion method, the gray area can be removed by setting h to a sufficiently small value in Eq. (2). However, the optimization analysis cannot proceed well with a fairly small h. Therefore, it is important to set an appropriate value of h to confirm the percentage of gray area occupied in the entire area of the design region. In our optimization, we set a large percentage of the gray area in the early stage of optimization, and it would decrease with the

#229351 - $15.00 USD Received 18 Dec 2014; revised 31 Jan 2015; accepted 1 Feb 2015; published 9 Feb 2015

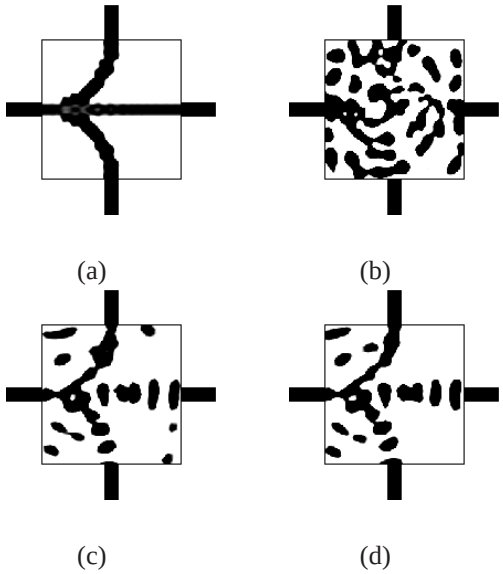

Fig. 3. 2-D topology optimization for the triplexer with the design region of $W_x = W_y = 2\ \mu$m: (a) the initial structure, the optimized structures based on (b) the Fourier series, (c) the sampling function, (d) the pyramid function.

optimized procedure. The optimization is performed in a larger area in the early stage, and the material boundary can be modified in the later stage of the optimization. Here, the h can be written as

$$h = h_{\max} \exp(-i/M) \tag{20}$$

where i is the number of iterations, M is a quantity representing the rate of decrease in h and we set $M = 50$ in this paper. $h_{\max}$ equals the value of h at the 0-th iteration step. Here, since the value of h decreases exponentially, h takes a fairly small value with the optimized procedure. In that case, we determine h to ensure that the percentage of gray area is less than a predetermined value. For example, in the optimization of the triplexer mentioned in the next section, in order to ensure the weakly waveguide in the early stage of the optimization design, the value of $h_{\max}$ is set to be $1 \sim 2$ times the maximum value of the initial function $\xi(x,y)$ in Eq. (1). This is because in the optimization design of a optical waveguide, a weakly waveguide problem has a low possibility to fall into a localized optimal solution.

3. Optimal design example of optical devices

3.1. Optimize the triplexer with $2\ \mu\text{m} \times 2\ \mu\text{m}$ *design region*

Here, we optimize a triplexer using the function-expansion-based topology optimization method described in the previous section.

The design problem is shown in Fig. 1. Assuming a beam of three-wavelength multiplexed light ($\lambda_1 = 1.31\ \mu$m, $\lambda_2 = 1.49\ \mu$m, $\lambda_3 = 1.55\ \mu$m) is launched into port 1, light of each wavelength separates into different ports through the optimized design region, *i.e.* $\lambda_1 = 1.31\ \mu$m emits from port 2, $\lambda_2 = 1.49\ \mu$m emits from port 3 and $\lambda_3 = 1.55\ \mu$m emits from port 4. The design region consists of only two kinds of materials and the refractive indices of core and cladding regions are $n_1 = 3.4$ and $n_2 = 1.45$, respectively. To achieve the single mode propagation for each wavelength, the input and output waveguides have the same width which

#229351 - $15.00 USD Received 18 Dec 2014; revised 31 Jan 2015; accepted 1 Feb 2015; published 9 Feb 2015

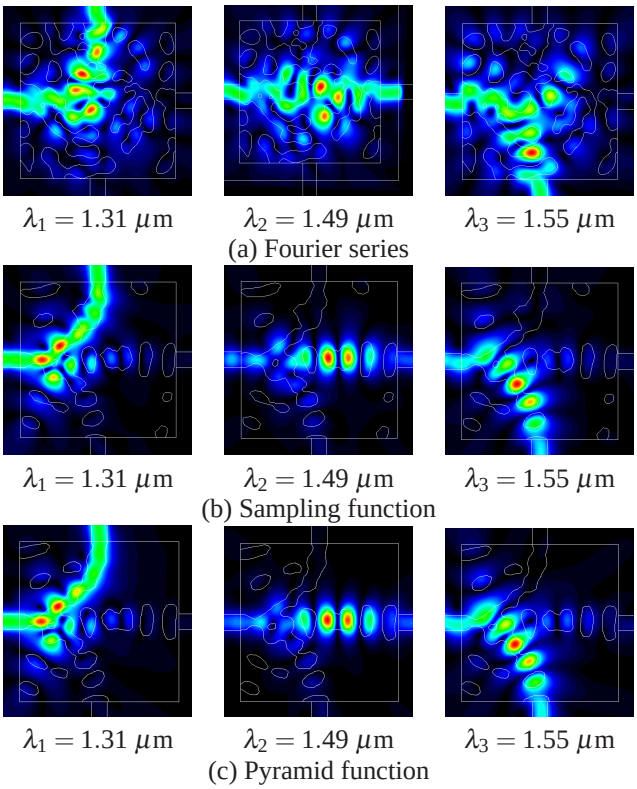

Fig. 4. The propagation behaviors of the optimized structure based on different functions ($W_x = W_y = 2\ \mu$m).

Table 1. The normalized transmission power of each optimized structure with the design region of $W_x = W_y = 2\ \mu$m.

	port 2 ($\lambda_1 = 1.31\ \mu$m)	port 3 ($\lambda_2 = 1.49\ \mu$m)	port 4 ($\lambda_3 = 1.55\ \mu$m)
Fourier	0.960	0.930	0.934
Sampling	0.948	0.884	0.904
Pyramid	0.947	0.886	0.886

is set to $w = 0.2\ \mu$m. The design region widths in x- and y-direction are, respectively, $W_x = W_y = 2\ \mu$m, the waveguide position is $d = 1\ \mu$m. The objective function to be maximized is given as follows:

$$C = \sum_{i=1}^{3} \left| S_{(i+1)1}(\lambda_i) \right|^2 . \tag{21}$$

Here, the numbers of the expansion functions along the x- and y-direction are $N_x = N_y = 16$, and the number of iteration steps is set to 500.

In order to compare the optimized results obtained by different expansion functions, we adopt a Fourier series, a sampling function and a pyramid function to express the structure of design region. The initial structure for the optimization and the optimized structures obtained by the three kinds of functions are illustrated in Fig. 3. Here, L_x and L_y are set to the same value 2.2 μm

#229351 - $15.00 USD Received 18 Dec 2014; revised 31 Jan 2015; accepted 1 Feb 2015; published 9 Feb 2015

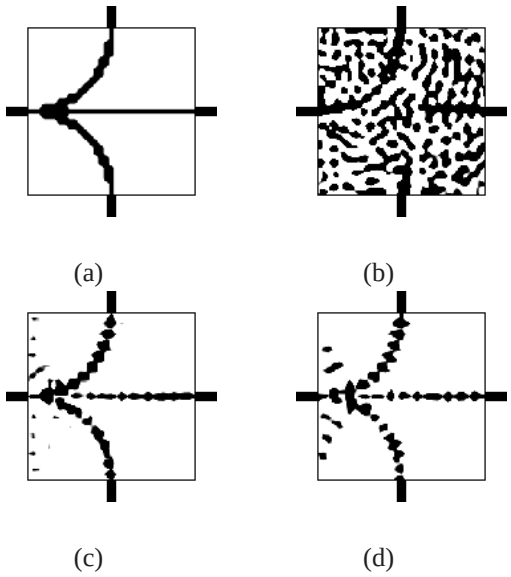

Fig. 5. 2-D topology optimization for the triplexer with the design region of $W_x = W_y = 4\ \mu$m: (a) the initial structure, the optimized structures based on (b) the Fourier series, (c) the sampling function, (d) the pyramid function.

in Eq. (5) for the analysis using Fourier series. The propagation behaviors of the optimized structure based on different functions are shown in Fig. 4. As for the three optimized structures, we can observe that the optimization structure obtained by the Fourier series has the most complicated distribution, and the structures obtained by the sampling function and the pyramid function have almost the same distributions which are simpler than that with the Fourier series. The normalized transmission power of each output waveguide is shown in Table 1. Comparing the normalized transmission power, the characteristics are degraded in the order of the Fourier series, the sampling function and the pyramid function. In addition, the characteristics based on the sampling function and the pyramid function are close to each other. However, the structure based on sampling function has a better property because it is easy to update the surrounding structures than the structure based on the completely localized pyramid function.

3.2. Optimize the triplexer with $4\ \mu\text{m} \times 4\ \mu\text{m}$ *design region*

We have optimized the triplexer with the design region of $W_x = W_y = 2\ \mu$m so far. Then in order to improve the characteristics of the optimized device by suppressing the radiation power, we optimize the separator with a larger design region. Here, the design region widths in x- and y-direction are set to $W_x = W_y = 4\ \mu$m, and the waveguide position is $d = 2\ \mu$m. Considering the wavelength bandwidth used in the actual communication, according to the international standards (TDM-PON ITU-T G.983 and G.984), we optimized the design region to separate the light of each wavelength bandwidth into different ports. Here, through the design region of the triplexer, $\lambda = 1.26 \sim 1.36\ \mu$m emit from port 2, $\lambda = 1.48 \sim 1.50\ \mu$m emit from port 3 and $\lambda = 1.55 \sim 1.56\ \mu$m emit from port 4. The other parameters are set as the same as the previous optimization in the smaller design region. Here, the objective function to be maximized is given as follows:

$$C = \sum_{i=1}^{3} \sum_{j=1}^{2} \left| S_{(i+1)1}(\lambda_{i,j}) \right|^2 \tag{22}$$

#229351 - $15.00 USD Received 18 Dec 2014; revised 31 Jan 2015; accepted 1 Feb 2015; published 9 Feb 2015

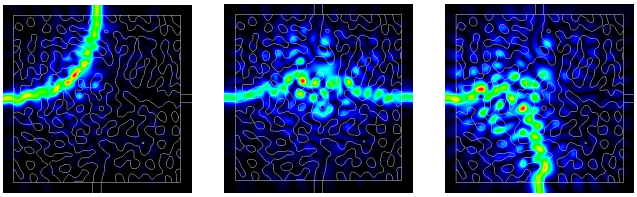

$\lambda_1 = 1.31\ \mu$m $\lambda_2 = 1.49\ \mu$m $\lambda_3 = 1.55\ \mu$m

(a) Fourier series

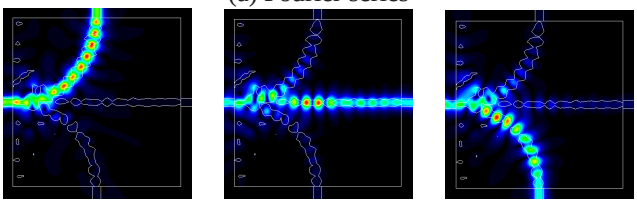

$\lambda_1 = 1.31\ \mu$m $\lambda_2 = 1.49\ \mu$m $\lambda_3 = 1.55\ \mu$m

(b) Sampling function

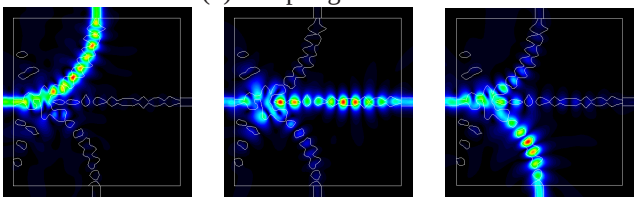

$\lambda_1 = 1.31\ \mu$m $\lambda_2 = 1.49\ \mu$m $\lambda_3 = 1.55\ \mu$m

(c) Pyramid function

Fig. 6. The propagation behaviors of the optimized structure based on different functions ($W_x = W_y = 4\ \mu$m).

Table 2. The normalized transmission power of each optimized structure with the design region of $W_x = W_y = 4\ \mu$m.

	port 2 ($\lambda_1 = 1.31\ \mu$m)	port 3 ($\lambda_2 = 1.49\ \mu$m)	port 4 ($\lambda_3 = 1.55\ \mu$m)
Fourier	0.997	0.999	0.997
Sampling	0.979	0.956	0.951
Pyramid	0.971	0.947	0.938

where $\lambda_{1,1} = 1.26\ \mu$m, $\lambda_{1,2} = 1.36\ \mu$m, $\lambda_{2,1} = 1.48\ \mu$m, $\lambda_{2,2} = 1.50\ \mu$m, $\lambda_{3,1} = 1.55\ \mu$m,$\lambda_{3,2} = 1.56\ \mu$m, respectively. The numbers of the expansion functions along the x- and y-direction are also set to $N_x = N_y = 16$ and the number of iteration steps is set to 500.

The initial structure for the optimization and the optimized structures obtained by the three kinds of functions are illustrated in Fig. 5. Here, we set $L_x = L_y = 4.2\ \mu$m in Eq. (5) for the analysis using Fourier series. The propagation behaviors of the optimized structure with different functions are shown in Fig. 6. Similarly in the smaller design region, the optimized structure based on the Fourier series has a complicated distribution, and the sampling function and the pyramid function have almost the same structures which are simpler than that with the Fourier series. The normalized transmission power of each output wavelength is shown in Table 2 and the wavelength dependence of the normalized transmission power at each port is also illustrated in Fig. 7. For the characteristics obtained by the Fourier series, the transmission power of each

#229351 - $15.00 USD Received 18 Dec 2014; revised 31 Jan 2015; accepted 1 Feb 2015; published 9 Feb 2015

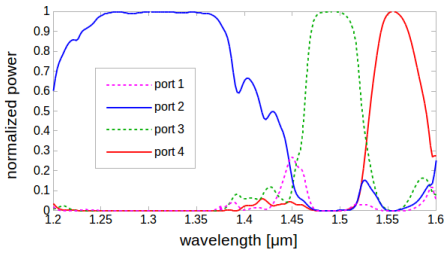

(a) Fourier series

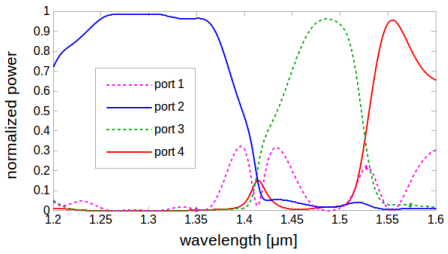

(b) Sampling function

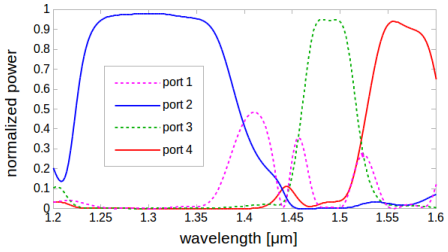

(c) Pyramid function

Fig. 7. Wavelength dependence of the normalized transmission power at each port for the optimized structure based on different functions ($W_x = W_y = 4\ \mu$m).

output wavelength band is almost 100% and the ideal properties can be obtained. By comparing the transmission power, characteristics are degraded in the order of the Fourier series, the sampling function and the pyramid function. According to Fig. 7(b), for the characteristics obtained by sampling function, we can observe that the normalized transmission power is higher than 95% in first band ($\lambda = 1.26 \sim 1.36\ \mu$m), 93% in the second band ($\lambda = 1.48 \sim 1.50\ \mu$m), and 94% in the third band ($\lambda = 1.55 \sim 1.56\ \mu$m). Similarly, for the characteristics obtained by pyramid function shown in Fig. 7(c), the normalized transmission power in each band is higher than 93%, 93% and 92%, respectively. From the above, it is observed that searching the global optimal region can obtain a better characteristic when we only consider the transmission power. However, we also note that the optimized structure based on the Fourier series has a much more complicated distribution than that obtained by the other two localized functions. Moreover, according to the wavelength dependences shown in Fig. 7, we can also observe that based on each expansion function, light of the wavelengths for each objective bandwidth is transmitted to the desired ports, respectively. In addition, the maximum crosstalk at each output port is investigated and shown in Table 3.

#229351 - $15.00 USD Received 18 Dec 2014; revised 31 Jan 2015; accepted 1 Feb 2015; published 9 Feb 2015

Table 3. The maximum crosstalk at each output port with the design region of $W_x = W_y = 4\ \mu$m.

	port 2 [dB]	port 3 [dB]	port 4 [dB]
Fourier	-26.3	-25.2	-22.6
Sampling	-17.2	-16.0	-15.0
Pyramid	-16.0	-13.8	-15.6

3.3. *Optimize the triplexer by considering material dispersion and waveguide thickness*

In the previous sections, we optimized the triplexer by adopting the material indices (Si and SiO_2) as constants for different wavelengths. However, in the actual materials, the material dispersion should be considered. In this section, we will optimize the triplexer with quasi 3-D topology optimization by considering the variation of material indices for different wavelengths. Referring to [19], we assuming the refractive index is isotropic and model the dispersion of silicon in core region using the Sellmeier model, shown as follows:

$$n_{\mathrm{Si}}^2 = \varepsilon_1 + \frac{A_1}{\lambda^2} + \frac{A_2\lambda_1^2}{\lambda^2 - \lambda_1^2} \tag{23}$$

where $\varepsilon_1 = 11.6858, A_1 = 0.939816, A_2 = 8.10461 \times 10^{-3}$ and $\lambda_1 = 1.1071\ \mu$m. The dispersion of silica in cladding is illustrated by the following equation:

$$n_{\mathrm{SiO_2}}^2 = 1 + \frac{B_1\lambda^2}{\lambda^2 - C_1} + \frac{B_2\lambda^2}{\lambda^2 - C_2} + \frac{B_3\lambda^2}{\lambda^2 - C_3} \tag{24}$$

where $B_1 = 0.69675$, $B_2 = 0.408218$, $B_3 = 0.890815$, $C_1 = 4.770112 \times 10^{-3}\ \mu\mathrm{m}^2$, $C_2 = 1.33777 \times 10^{-2}\ \mu\mathrm{m}^2, C_3 = 98.021069\ \mu\mathrm{m}^2$. The refractive indices of Si and SiO_2 as a function of wavelength are shown in Fig. 8. It can be observed that the indices vary slightly while the wavelength varies from 1.2 μm to 1.6 μm.

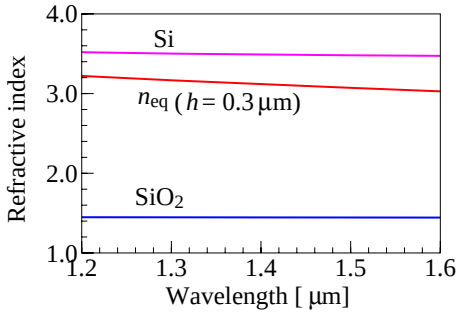

Fig. 8. Refractive indices of materials and equivalent core index used in EIM as a function of wavelength.

According to section 3.2, we note that the optimized structure obtained by sampling function is much simpler than that obtained by Fourier series. Moreover, the characteristics obtained by sampling function are better than that obtained by pyramid function. Therefore, we optimize the triplexer with quasi 3-D topology optimization based on the sampling function-expansion method. Here, we considering the thickness of each ports as $h = 0.3\ \mu$m instead of infinite

#229351 - $15.00 USD Received 18 Dec 2014; revised 31 Jan 2015; accepted 1 Feb 2015; published 9 Feb 2015

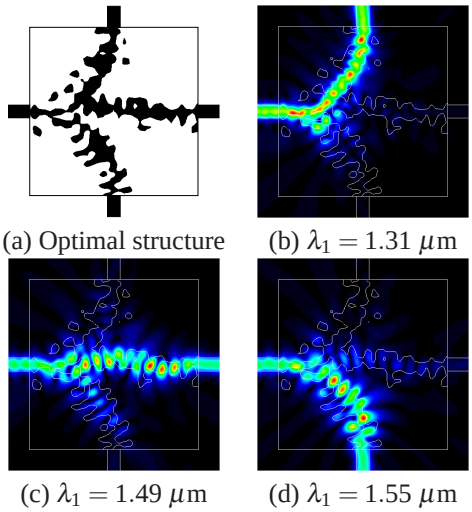

Fig. 9. Quasi 3-D topology optimization based on sampling function for the triplexer with the design region of $W_x = W_y = 4\ \mu$m: (a) the optimal structure, (b)∼(d) the propagation behaviors for each wavelength.

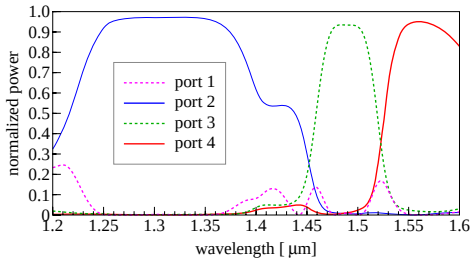

Fig. 10. Wavelength dependence of the normalized transmission power at each port for the optimized structure based on quasi 3-D topology optimization with sampling functions ($W_x = W_y = 4\ \mu$m).

thickness along the *y*-direction in 2-D topology optimization. To achieve single-mode propagation for each wavelength, the widths of input and output waveguides are set to $w = 0.3\ \mu$m. Other parameters are set as the same as those in section 3.2. In this example, TE-like mode is considered as the incident mode and the effective index method (EIM) is used to reduce the 3-D model to the 2-D model. The dispersion curve of the equivalent core index of the EIM, n_{eq}, is illustrated in Fig. 8.

The optimized structure and the propagation behaviors for each wavelength are shown in Fig. 9. The wavelength dependence of the normalized transmission power at each port is shown in Fig. 10. It can be seen that the normalized transmission power is higher than 95% in the first band ($\lambda = 1.26 \sim 1.36\ \mu$m), 92% in the second band ($\lambda = 1.48 \sim 1.50\ \mu$m), and 94% in the third band ($\lambda = 1.55 \sim 1.56\ \mu$m). The maximum crosstalks for output ports 2 to 4 are -24.0 dB, -16.0 dB and -16.0 dB, respectively. Compared with the optimal structure obtained by 2-D topology optimization based on sampling function, the structure with quasi 3-D method has a relatively complex distribution, and the normalized transmission power decrease slightly for each wavelength band. However, the crosstalk between the wavelengths is much more suppressed, especially in port 2 and port 4.

#229351 - $15.00 USD Received 18 Dec 2014; revised 31 Jan 2015; accepted 1 Feb 2015; published 9 Feb 2015

4. Conclusion

In this paper, in order to optimize the photonic devices by using the function-expansion-based topology optimization method, we adopted the Fourier series, the sampling function and the pyramid function as the expansion functions to express the refractive index distribution in the design region. The examples of optimal design demonstrated that the optimized structure based on the Fourier series has high characteristic but with a complicated distribution. On the other hand, the optimized structures based on the sampling function and the pyramid function have almost the same distributions which are simpler than that with the Fourier series, however, the characteristics are slightly lower than that obtained by the Fourier series. Since the reciprocity, our proposed triplexer can achieve bidirectional transmission, *i.e.* one wavelength band for upload ($\lambda = 1.26 \sim 1.36$ μm) and two bands for download ($\lambda = 1.48 \sim 1.50$ μm and $\lambda = 1.55 \sim 1.56$ μm).

We have optimized the triplexer by using 2-D and quasi 3-D topology optimization so far, in the future, we will continue optimizing the optical circuit device with 3-D topology optimization in detail.

Acknowledgment

The authors would like to thank S. Kato for his valuable work.

#229351 - $15.00 USD Received 18 Dec 2014; revised 31 Jan 2015; accepted 1 Feb 2015; published 9 Feb 2015